

## Research Article

# Density Functional Theoretical Computational Studies on 3-Methyl 2-Vinyl Pyridinium Phosphate

N. Kanagathara <sup>1</sup>, V. J. Thanigaiarasu,<sup>2</sup> V. Sabari,<sup>3</sup> and S. Elangovan <sup>4</sup>

<sup>1</sup>Department of Physics, Saveetha School of Engineering, Saveetha Institute of Medical and Technical Sciences, Thandalam, Chennai-602 105, India

<sup>2</sup>Department of Physics, Jaya Arts and Science College, Thiruninravur, Chennai-602024, India

<sup>3</sup>Department of Physics, Marudhar Kesari Jain College for Women, Vaniyambadi, Tamilnadu-635 751, India

<sup>4</sup>Department of Physics, College of Natural and Computational Sciences, Wollega University, Nekemte-395, Ethiopia

Correspondence should be addressed to S. Elangovan; [elangovan.physics@rediffmail.com](mailto:elangovan.physics@rediffmail.com)

Received 3 May 2022; Revised 14 July 2022; Accepted 28 July 2022; Published 18 August 2022

Academic Editor: Sefer Bora Lisesivdin

Copyright © 2022 N. Kanagathara et al. This is an open access article distributed under the Creative Commons Attribution License, which permits unrestricted use, distribution, and reproduction in any medium, provided the original work is properly cited.

The molecular structure of 3-methyl 2-vinyl pyridinium phosphate (3M2VPP) has been optimized by using Density Functional Theory using B3LYP hybrid functional with 6-311++G (d, p) basis set in order to find the whole characteristics of the molecular complex. The theoretical structural parameters such as bond length, bond angle, and dihedral angle are determined by DFT methods and are well agreed with the single crystal X-ray diffraction parameters. Theoretical vibrational, highest occupied molecular orbital - lowest unoccupied molecular orbital (HOMO-LUMO), natural bonding orbital (NBO), and electrostatic potential (ESP) analyses have also been performed. Based on the potential energy distribution (PED), the complete vibrational assignments, analysis, and correlation of the compound's fundamental modes have been determined. Natural bonding orbital (NBO) analysis is used to evaluate the intramolecular charge transfer and hyper-conjugative interaction of the molecule. B3LYP/6-311++G (d, p) basis set determines the electronic properties such as HOMO-LUMO energies and is used to understand the kinetic stability and chemical reactivity of the studied compound. Molecular electrostatic potential (MEP) is used to investigate the electron density distribution and chemical reactive sites of 3M2VPP. The dipole moment, total polarizability, and the first-order hyperpolarizability calculations have been carried out for the studied molecule. Hirshfeld surface analysis has been done to study the intermolecular interactions in the studied complex.

## 1. Introduction

Organic aromatic materials with the ability of charge transfer have attracted many researchers for the past two decades and have been recognized as a material for the development of nonlinear optical materials [1, 2]. Organic phosphates are highly lustrous, adherent, and ductile, and their additives are used in electroplating baths. Structure, as well as biological activities of thiazolo-pyridine dicarboxylic derivatives, were reported by Yahia et al. [3]. Linear, as well as nonlinear optical properties of pyridine N-oxide, were reported by Sosun et al. [4]. Phosphoric acid pyridine-1-ium-2-carboxylate has been identified as a potential

nonlinear optical material and is useful for device fabrication [5]. There are many reports available for the pyridine derivatives applications in the nonlinear optical field [6–10]. Pyridinium salts and its derivatives are found in various natural and bioactive compounds [11]. It has wide applications such as acylating agents and phase transfer catalysts and has found use in industrial applications such as dyes, surfactants, cosmetics, pharmaceuticals, polymerization, phase transfer agents, catalysis, sensors, and electrolytes [12]. In continuation of research on possible and potential applications of pyridine and its salts, the present study is aimed to study the quantum chemical computations of 3-methyl 2-vinyl pyridinium phosphate. The structure of 3-methyl 2-

vinyl pyridinium phosphate was reported by Kalaiselvi et al. [13]. The title crystal crystallizes in a monoclinic system having a  $P2_1/c$  space group with lattice parameters  $a = 7.7089$  (6) Å,  $b = 16.366$  (13) Å,  $c = 8.0649$  (6) Å,  $\alpha = 90^\circ$ ,  $\beta = 109.689$  (4) $^\circ$ ,  $\gamma = 90^\circ$  and  $V = 958.06$  (13) Å<sup>3</sup>. The 3-methyl 2-vinyl pyridinium cations are bonded to phosphate anions via N-H...O and C-H...O interactions [13]. In the present communication, the optimized geometry, vibrational, NBO, and other electronic parameters have been discussed theoretically with DFT/B3LYP-6-311++G (d, p) basis set.

## 2. Materials and Methods

**2.1. Synthesis of 3-Methyl 2-Vinyl Pyridinium Phosphate.** 1 g (0.0084 mol) of freshly distilled 3-methyl,2-vinyl pyridine was dissolved in 15 mL of diethyl ether at  $-10^\circ\text{C}$  under a nitrogen atmosphere. To the above solution, 0.5 mL of  $\text{H}_3\text{PO}_4$  and 10 mL of diethyl ether mixture were added in drops with continuous stirring. The product obtained as a white solid was filtered, washed with diethyl ether, and dried under a vacuum, the product was recrystallized from methanol. Yield: 100% (1.82 g) [13].

## 3. Results and Discussion

**3.1. Structural Analysis.** The molecular structure along with the numbering of atoms of 3-methyl 2-vinyl pyridinium phosphate is obtained from Gaussian 09 and GaussView programs and is shown in Figure 1. [14, 15]. The most optimized structural parameters (bond length and bond angle) are calculated by B3LYP/6-311++G (d, p) basis sets are compared with experimental data from the results the bond lengths and angles have normal values. The asymmetric unit is composed of one 3-methyl 2-vinyl pyridinium cation and one phosphate anion. The C1—N1—C5 angle in the pyridinium ring is widened to 123.35 (2) $^\circ$ , compared to 115.25 (13) $^\circ$  in 4-aminopyridine, 121.20 (15) $^\circ$  in 1-(2-carboxy-ethyl)-5-ethyl-2-methylpyridinium and 120.7 (2) $^\circ$  in Aminopyridinium. The 3-methyl 2-vinyl pyridinium ring is essentially planar with the maximum deviation from planarity being 0.008 (2) Å for atom C5. The sum of the bond angles around the N1 atom (359.89 $^\circ$ ) indicates sp<sup>2</sup> hybridization. The phosphate anions form centrosymmetric R<sub>2</sub><sup>2</sup> (8) dimers via O—H...O hydrogen bonds. These dimers are further linked to chains running along the  $c$  axis. The cations are bonded to the anions via N—H...O hydrogen bonds and C—H...O contacts [13]. Table 1 list the geometric parameters of 3M2VPP. Theoretically computed bond distance and bond angles are very well matches with experimentally observed geometric parameters.

**3.2. Vibrational Analysis.** The analytical techniques of infrared (IR) absorption and Raman spectroscopy are frequently utilised in the quest for novel materials. Experimental methods become even better adopted for the complexity of highly functionalized materials when combined with the strength of recent computational chemistry technologies. The computational element aids in the analysis of the data-rich spectroscopic results, while the latter also

confirms the computational approach used. The title molecule has 26 atoms and has 72 (3N-6) normal modes of vibration. The theoretically constructed FT-IR and FT Raman spectrum is shown in Figure 2. The vibrational frequencies obtained using the B3LYP method with the standard 6-311++G (d, p) basis set calculations together with the approximate description of each normal mode are tabulated in Table 2.

### 3.2.1. 3-Methyl 2-Vinyl Pyridinium Cation Vibrations.

2-vinylpyridine is a polymer that is extensively utilised in the fabrication of multilayer films and as a matrix for the embedding of semiconductor nanoparticles. It exhibits unique photochemical properties as a result of the lone pair of sp<sup>2</sup> electrons, leading to a variety of applications such as pH-responsive coatings. Absorption bands due to the stretching modes of CH and CH<sub>2</sub> groups can be seen in the frequency range of 2800–3200 cm<sup>-1</sup>. The variations in this spectral region were obvious but modest since the molar strength of the CH stretching vibration is quite small. The loss of methyne protons in the 2-vinyl pyridine structure was blamed for the reduction of strength in the methyne bands at 3010–3030 cm<sup>-1</sup> in the gel spectrum. The NH<sup>+</sup> stretching vibration of the pyridinium ion was attributed to a new, very strong infrared band at 3400 cm<sup>-1</sup> [16]. Theoretically, these peaks are computed at 3120–2930 cm<sup>-1</sup>. The computed peak at 1880 cm<sup>-1</sup> is attributed to N-H in-plane bending vibration. According to PED calculations, there are weak peaks observed in the range 1150–1029 cm<sup>-1</sup> and are attributed to C-C-H bending vibrations. The torsional vibrations of HCCC are computed in the region 980–950 cm<sup>-1</sup> with weak infrared and Raman intensity except at 953 cm<sup>-1</sup> with strong infrared intensity. 1630–1510 cm<sup>-1</sup> range of frequencies are ascribed to C-C stretching vibrations of the 2-vinylpyridine ring. Methyl group bending vibrations are calculated at 1462 and 1440 cm<sup>-1</sup>. Similar peaks were observed at 1375 and 1372 cm<sup>-1</sup> with medium intensity. The other peak vibrations are computed and provided in Table 2.

**3.2.2. Phosphate Anion Vibrations.** Phosphate anion includes vibrations of PO<sub>4</sub> stretching as well P-O-H bending mode. The internal vibrations of each H<sub>2</sub>PO<sub>4</sub><sup>-</sup> ion are divided into vibrations of the two groups, PO<sub>2</sub> and P(OH)<sub>2</sub> which is due to the presence of two P-OH longer bonds and P-O shorter bonds [17, 18]. PED computed values at 3710 and 3708 cm<sup>-1</sup> is contributed to O-H asymmetric stretching vibrations of a phosphate anion. The stretching vibrations of the P-O bonds are theoretically computed at 1194, 1180, 1015, 985, 820, 812, 793, and 774 cm<sup>-1</sup>. P-O<sub>2</sub> asymmetric stretching ranges from 1060 to 1175 cm<sup>-1</sup> whereas symmetric stretching ranges from 1035 to 1065 cm<sup>-1</sup>. Asymmetric stretching vibrations of P(OH)<sub>2</sub> lie in the region 950–980 cm<sup>-1</sup> and symmetric stretching vibrations of P(OH)<sub>2</sub> are in the region 900 to 920 cm<sup>-1</sup>. This type of P-O stretching bond is experimentally found at 1175 and 900 cm<sup>-1</sup> [19, 20].

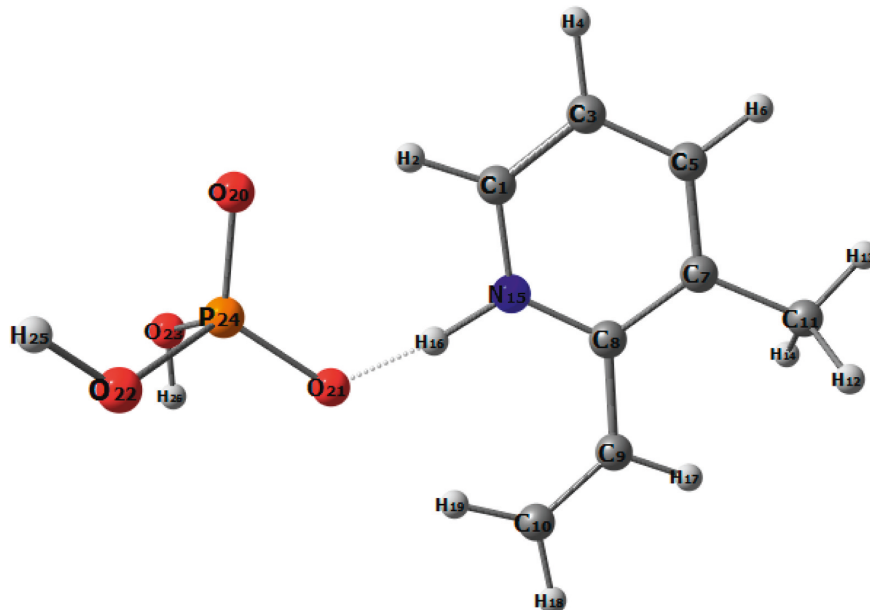


FIGURE 1: Optimized structure 3M2VPP.

**3.3. Natural Bonding Orbitals Analysis.** NBOs analysis gives deep insight into the chemical bonding of all the complexes. It also makes available substantial information regarding the nature of bonding orbitals, their occupancies as well as the type and nature of the interaction (intermolecular or intramolecular, hyper-conjugative or charge transfer) existing between virtual and occupied Lewis orbitals. The analysis is conducted by considering all probable interactions between donor (occupied Lewis NBOs) and acceptors (vacant) non-Lewis NBOs, and approximating their energetic significance by second-order perturbation theory of the Fock matrix [21, 22]. For this analysis, all potential interactions between “full” (donor) Lewis-type NBOs and “empty” (acceptor) non-Lewis NBOs are examined, and their energy significance is estimated using second-order perturbation theory. These interactions are known as “delocalization” corrections to the zeroth-order natural Lewis structure because they cause a loss of occupancy from the localised NBOs of the idealised Lewis structure into the empty non-Lewis orbitals (and thus, to departures from the idealised Lewis structure description) [23]. In the present study, donor-acceptor interactions were applied for investigating interactions in the 3M2VPP molecular complex. Table 3 shows some of the significant donor-acceptor interactions and their stabilization energies  $E^{(2)}$ . The NBO charges on the particular atoms computed for 3M2VPP are shown in Table 3. According to the calculation, the methyl group attached carbon atom in the pyridine ring (7C) have smaller negative charges ( $-0.598e$ ) than the carbon atom (10C) in the  $\text{CH}_2$  groups ( $-0.265e$ ). The nitrogen atom (15N) of the pyridine ring which is involved in hydrogen bonds (H16) shows the highest positive charge  $0.4765e$  confirms the occurrence of protonation. For singly protonated 2-vinyl pyridinium cation, the most charge difference i.e.,  $-0.466e$  is observed at 15N where the proton is attached. The methyl group hydrogen atoms (12H, 13H, and 14H) have higher

similar positive charges ( $0.215e$  to  $0.222e$ ) than the other hydrogen atoms (18H and 19H) of the C-H groups. The calculated charges for carbon atoms C1, C3, C5, C7, and C8 in the pyridine ring are completely different. The adjacent carbon atoms 1C and 8C carry positive charges whereas 3C, 5C, 7C, and 8C have negative charges. The phosphorus atom (24P) has a more positive charge of  $2.471e$  and all the oxygen atoms have negative charges. Hydrogen atoms 25H and 26H have more positive charges. Thus, the positive and negative charges are balanced and establishes the stability of the molecule as shown in Figure 3. The donor-acceptor interactions of the inclusion complex of phosphoric acid into 3-methyl 2-vinyl pyridine are investigated using the NBO program. The obtained results are illustrated in Table 3. The interaction energies of these contacts are in the range of  $4\text{--}363\text{ kJmol}^{-1}$ . The highest intramolecular stabilization energy of  $91.12\text{ kJmol}^{-1}$  is found in 3-methyl-2-vinylpyridine between antibonding  $\pi$  orbitals of C1-N15 to C3-C5. The next highest stabilization energy is due to the lone pair of carbon atom C7 with  $\pi^*(\text{C3-C5})\text{--}71.58\text{ kJmol}^{-1}$  and C8 with  $\pi^*(\text{C1-N15})\text{--}67.09\text{ kJmol}^{-1}$ . The strongest intermolecular stabilization energy occurs in between the lone pair of electronegative nitrogen atom N15 in 3-methyl-2-vinyl pyridine to H16 in phosphoric acid establishing energy of  $362.82\text{ kJmol}^{-1}$ . The lone pair of oxygen atom O21 with antibonding H16 has  $14.13\text{ kJmol}^{-1}$  confirming the protonation between the molecules. Intramolecular stabilization energy of phosphoric acid lies in the range of  $10$  to  $22\text{ kJmol}^{-1}$  [24, 25]. The other type of intermolecular and intramolecular interactions and their energies are tabulated in Table 3.

**3.4. Frontier Molecular Orbitals (FMOs) Analysis.** Frontier molecular orbitals (FMO) theory allows a chemist to make predictions about a reaction by knowing the

TABLE 1: Selected bond parameters of 3M2VPP.

Atom	Bond distance (Å)	
	Calculated	Expt.
1C-2H	1.09	1.029
1C-3C	1.3838	1.372
1C-15N	1.3418	1.334
3C-4H	1.0817	0.930
3C-5C	1.3909	1.384
5C-6H	1.0849	0.930
5C-7C	1.396	1.389
7C-8C	1.411	1.396
7C-11C	1.5089	1.502
8C-9C	1.466	1.468
8C-15N	1.3549	1.351
9C-10C	1.3392	1.294
9C-17H	1.0829	0.992
10C-18H	1.0841	1.064
10C-19H	1.0849	1.020
11C-12H	1.0934	0.960
11C-13H	1.0907	0.960
11C-14H	1.0936	0.960
15N-16H	1.1255	1.089
16H-21O	1.4116	1.412
20O-24P	1.4939	1.492
21O-24P	1.5344	1.512
22O-24P	1.6384	1.647
22O-25H	0.9641	0.880
23O-24P	1.6341	1.589
23O-26H	0.964	0.889

Atom	Bond angle (°)	
	Calculated	Expt.
2H-1C-3C	124.9693	119.94
2H-1C-15N	115.0102	119.94
3C-1C-15N	120.0187	120.11
1C-3C-4H	119.9727	120.79
1C-3C-5C	118.3786	118.38
4H-3C-5C	121.6486	120.83
3C-5C-6H	119.6955	119.31
3C-5C-7C	121.4081	121.32
6H-5C-7C	118.8962	118.37
5C-7C-8C	117.9677	118.05
5C-7C-11C	120.1661	120.77
8C-7C-11C	121.8654	121.89
7C-8C-9C	121.6164	120.57
7C-8C-15N	118.7077	118.76
9C-8C-15N	119.6758	118.66
8C-9C-10C	126.7544	126.99
8C-9C-17H	114.6652	115.28
10C-9C-17H	118.5775	117.68
9C-10C-18H	119.1689	119.09
9C-10C-19H	123.6603	121.74
18H-10C-19H	117.1705	113.19
7C-11C-12H	111.6949	109.52
7C-11C-13H	110.3074	109.39
7C-11C-14H	111.722	109.40
12H-11C-13H	107.7316	109.46
12H-11C-14H	107.532	109.52
13H-11C-14H	107.667	109.48
1C-15N-8C	123.5167	123.35
1C-15N-16H	113.4781	112.90

TABLE 1: Continued.

8C-15N-16H	123.0017	123.64
16H-21O-24P	118.5485	120.19
24P-22O-25H	110.5635	110.92
24P-23O-26H	111.5211	111.91
20O-24P-21O	119.1096	119.20
20O-24P-22O	111.7533	110.92
20O-24P-23O	108.9413	107.45
21O-24P-22O	104.5152	106.04
21O-24P-23O	107.7098	108.56
22O-24P-23O	103.6473	106.43

Atom	Dihedral angle (°)	
	Calculated	Expt.
2H-1C-3C-4H	-0.4648	-1.14
2H-1C-3C-5C	179.587	178.91
15N-1C-3C-4H	-179.955	178.84
15N-1C-3C-5C	0.0969	-1.12
2H-1C-15N-8C	-179.197	-179.92
2H-1C-15N-16H	1.4626	-3.74
3C-1C-15N-8C	0.342	-0.05
3C-1C-15N-16H	-178.999	-176.28
1C-3C-5C-6H	179.8694	178.82
1C-3C-5C-7C	-0.2714	1.12
4H-3C-5C-6H	-0.078	1.18
4H-3C-5C-7C	179.7813	-178.06
3C-5C-7C-8C	0.0292	0.01
3C-5C-7C-11C	-179.666	-179.90
6H-5C-7C-8C	179.8895	179.99
6H-5C-7C-11C	0.1947	0.09
5C-7C-8C-9C	-179.461	178.17
5C-7C-8C-15N	0.3859	-1.16
11C-7C-8C-9C	0.2286	-1.02
11C-7C-8C-15N	-179.925	-178.76
5C-7C-11C-12H	119.7356	120.93
5C-7C-11C-13H	-0.048	-1.00
5C-7C-11C-14H	-119.768	-119.03
8C-7C-11C-12H	-59.9471	-60.89
8C-7C-11C-13H	-179.731	-179.01
8C-7C-11C-14H	60.5493	-60.89
7C-8C-9C-10C	175.3397	166.29
7C-8C-9C-17H	-4.0309	11.40
15N-8C-9C-10C	-4.5055	13.03
15N-8C-9C-17H	176.1239	-169.22
7C-8C-15N-1C	-0.5862	1.22
7C-8C-15N-16H	178.6925	174.73
9C-8C-15N-1C	179.2634	178.14
9C-8C-15N-16H	-1.4579	5.92
8C-9C-10C-18H	-179.652	179.40
8C-9C-10C-19H	0.5768	-0.47
17H-9C-10C-18H	-0.3029	-1.04
17H-9C-10C-19H	179.9254	178.17
16H-21O-24P-20O	6.2535	23.55
16H-21O-24P-22O	-119.362	-120.43
16H-21O-24P-23O	130.8515	144.66
25H-22O-24P-20O	35.222	40.28
25H-22O-24P-21O	165.3396	167.40
25H-22O-24P-23O	-81.9411	-78.66
26H-23O-24P-20O	169.2019	160.89
26H-23O-24P-21O	38.6974	34.80
26H-23O-24P-22O	-71.6849	-79.92

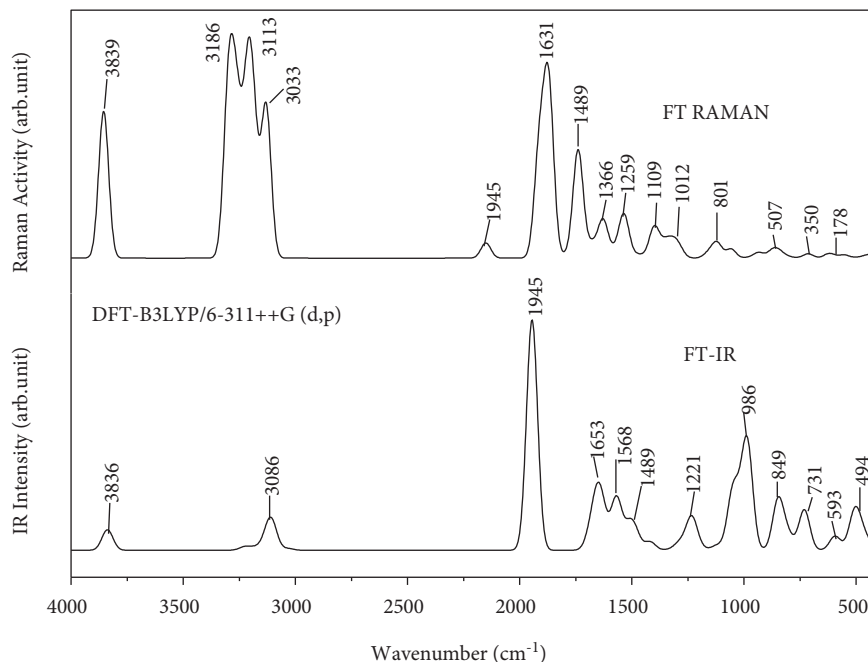


FIGURE 2: Theoretical FT-IR and FT Raman spectrum of 3M2VPP.

TABLE 2: Wave numbers ( $\text{cm}^{-1}$ ) and relative intensities of observed and calculated Fourier infrared and Raman spectra of 3M2VPP.

Unscaled frequency ( $\text{cm}^{-1}$ )	Scaled frequency ( $\text{cm}^{-1}$ )	IR intensity	Raman activity	Band assignment description (PED (%))
3839.231	3710.616	51.2159	140.5984	$\nu_{\text{asym}}$ (O-H) (54)
3836.701	3708.171	100.7144	66.9707	$\nu_{\text{asym}}$ (O-H) (46)
3226.976	3118.872	23.9205	91.6865	$\nu_{\text{asym}}$ (O-H) (95)
3213.225	3105.581	0.9295	160.0995	$\nu_{\text{asym}}$ (C-H) (96)
3186.801	3080.043	14.3401	75.7115	$\nu_{\text{asym}}$ (C-H) (96)
3172.228	3065.958	7.1712	112.926	$\nu_{\text{asym}}$ (C-H) (93)
3130.385	3025.517	59.4681	131.9634	$\nu_{\text{asym}}$ (C-H) (54)
3113.99	3009.671	11.5332	61.8349	$\nu_{\text{sym}}$ (C-H) (50)
3107.247	3003.154	187.0633	104.438	$\nu_{\text{sym}}$ (C-H) (82)
3086.252	2982.862	8.3904	66.7826	$\nu_{\text{sym}}$ (C-H) (49)
3033.515	2931.893	12.621	211.6118	$\nu_{\text{sym}}$ (C-H) (42)
1945.218	1880.054	1707.747	21.352	$\delta$ (N-H) (51)
1683.489	1627.092	115.4109	127.6561	$\nu$ (C-C) (32)
1653.911	1598.505	309.363	72.1817	$\nu$ (C-C) (20)
1631.208	1576.562	205.1555	200.4535	$\nu$ (C-C) (15)
1568.863	1516.306	385.1027	2.6362	$\nu$ (C-C) (32)
1513.435	1462.735	136.0634	10.9424	$\delta$ (H-C-H) (12)
1490.256	1440.332	9.4869	9.7149	$\delta$ (H-C-H) (13)
1489.437	1439.541	56.1753	72.3044	$\delta$ (H-C-H) (13)
1484.967	1435.22	57.956	65.349	$\nu$ (P-O) (26)
1422.962	1375.293	1.3854	12.4871	$\delta$ (H-C-H) (23)
1419.755	1372.193	61.5637	6.5647	$\delta$ (H-C-C) (13)
1366.921	1321.129	0.6227	51.4184	$\nu$ (C-C) (16)
1332.972	1288.318	4.6526	7.6211	$\nu$ (C-N) (12)
1287.937	1244.791	53.2241	10.7206	$\nu$ (C-N) (15)
1259.907	1217.7	7.5617	56.5216	$\nu$ (C-C) (12)
1236.001	1194.595	199.4374	0.9401	$\nu$ (P-O) (58)
1221.539	1180.617	53.9898	0.2654	$\nu$ (P-O) (26) (/ $\tau$ (H-N-C-C) (36)
1190.452	1150.572	9.9319	4.8839	$\delta$ (H-C-C) (10)
1128.714	1090.902	19.9676	6.2068	$\delta$ (H-C-C) (16)
1109.189	1072.031	19.5795	39.2419	$\delta$ (H-C-C) (12)
1065.315	1029.627	0.7481	0.8269	$\delta$ (H-C-C) (39)
1063.82	1028.182	7.2998	7.8261	$\delta$ (H-N-C) (11)

TABLE 2: Continued.

Unscaled frequency ( $\text{cm}^{-1}$ )	Scaled frequency ( $\text{cm}^{-1}$ )	IR intensity	Raman activity	Band assignment description (PED (%))
1050.696	1015.498	371.2096	12.7771	$\nu(\text{P-O})$ (16)
1035.493	1000.804	50.8985	1.6426	$\tau(\text{H-C-C-C})$ (18)
1032.588	997.9965	0.8575	0.3042	$\tau(\text{H-C-C-C})$ (40)
1019.36	985.2112	91.8015	5.831	$\nu(\text{P-O})$ (15) $\delta(\text{H-O-P})$ (13)
1012.457	978.5396	4.4746	5.3341	$\tau(\text{H-C-C-C})$ (31)
1010.606	976.7502	24.3593	7.459	$\tau(\text{H-C-C-C})$ (39)
986.0833	953.0495	255.5356	3.7348	$\tau(\text{H-C-C-C})$ (35)
984.8057	951.8147	517.784	6.6565	$\tau(\text{H-C-C-C})$ (16)
849.3175	820.8654	322.5763	2.467	$\nu(\text{P-O})$ (50)
840.6951	812.5318	46.9717	4.622	$\nu(\text{P-O})/\delta(\text{C-C-C})$ (14)
821.4817	793.9621	26.9244	0.5279	$\nu(\text{P-O})$ (38)/ $\delta(\text{C-C-C})$ (17)
801.2227	774.3817	76.5963	20.3339	$\nu(\text{P-O})$ (42)
797.2224	770.5154	11.4183	1.1044	$\tau(\text{H-C-C-C})$ (13)/ $\tau(\text{C-N-C-C})$ (28)
731.3239	706.8245	299.7105	12.8903	$\nu(\text{C-C})$ (11)
638.8264	617.4257	0.0743	1.1833	$\tau(\text{H-C-C-C})$ (19)/ $\tau(\text{C-N-C-C})$ (15)
593.9972	574.0983	104.4292	7.774	$\delta(\text{H-N-C})$ (14)
531.8615	514.0441	16.4713	7.2788	$\nu(\text{C-C})$ (15)
507.6132	490.6082	206.5732	5.752	$\omega(\text{O-H})/\omega(\text{O-P-O})$ (16)
497.2902	480.631	51.7388	1.9153	$\delta(\text{H-O-P})$ (11)
494.3387	477.7784	16.5827	1.6197	$\omega(\text{H-O-P})$ (11)/ $\tau(\text{H-C-C-C})$ (10)
483.3281	467.1366	50.6303	2.0877	$\tau(\text{O-O-O-P})$ (26)
456.1658	440.8842	66.6765	1.7577	$\tau(\text{O-O-O-P})$ (27)
442.7693	427.9365	3.9289	0.4109	$\tau(\text{O-O-O-P})$ (18)
406.9055	393.2742	7.602	0.4082	$\tau(\text{H-O-P-O})$ (24)
350.1837	338.4525	5.3613	4.5604	$\tau(\text{H-O-P-O})$ (19)
344.8172	333.2658	8.1188	1.7445	$\omega(\text{O-O-O-P})$ (19)
277.187	267.9012	74.5551	0.1594	$\tau(\text{C-C-C-C})$ (25)/ $\tau(\text{H-O-P-O})$ (41)
261.6002	252.8366	3.365	0.6734	$\tau(\text{C-C-C-C})$ (12)/ $(\text{C-C-N-C})$ (20)
245.9159	237.6777	0.5094	5.0403	$\tau(\text{C-N-H-O})$ (20)
220.2828	212.9033	192.3981	1.6911	$\tau(\text{H-O-P-O})$ (30)
178.0645	172.0993	2.4475	0.8118	$\tau(\text{C-C-N-C})$ (14)/ $\tau(\text{O-O-O-P})$ (13)
173.0998	167.301	20.3573	1.6346	$\tau(\text{C-C-N-C})$ (14)/ $\tau(\text{O-O-O-P})$ (13)
166.1433	160.5775	3.3157	2.0295	$\tau(\text{H-C-C-C})$ (16)
120.4188	116.3848	7.9522	0.4634	$\tau(\text{H-N-C-C})$ (13)/ $\tau(\text{C-C-C-C})$ (14)
94.6788	91.50706	0.588	0.4054	$\tau(\text{C-C-C-N})$ (27)
87.8298	84.8875	0.4609	0.379	$\tau(\text{C-C-C-N})$ (45)
62.5897	60.49295	2.4308	2.2013	$\tau(\text{H-O-P-O})$ (10)
36.5715	35.34635	0.6811	2.168	$\tau(\text{C-N-H-O})$ (20)
28.0033	27.06519	2.5026	1.8538	$\tau(\text{C-N-H-O})$ (72)

placement of the HOMO and LUMO energy levels. Fukui developed the frontier molecular orbital theory to explain the chemical reactivity of the sample [26]. The Frontier molecular orbitals such as HOMO and LUMO affords information about the chemical stability and electrical and optical properties of the compounds; also it is used to explain various types of reactions in conjugated systems. The HOMO-LUMO orbitals are referred to as frontier molecular orbitals (FMOs) as they lie at the outermost boundaries for the electrons in a system. The pictorial representations of HOMO and LUMO orbitals have been calculated by using the B3LYP/6-311++G (d, p) basis set as depicted in Figure 4. HOMO is completely occupied in the 3-methyl 2-vinyl pyridinium ring and LUMO is partially occupied in the 3-methyl 2-vinyl pyridinium ring which seems that the majority of interaction takes place within the ring. The calculated energy values of HOMO and LUMO in 3-methyl 2-vinyl pyridinium phosphate are  $-9.987 \text{ eV}$  and  $-6.443 \text{ eV}$  and

the frontier orbital energy gap value is  $3.544 \text{ eV}$  as listed in Table 4. HOMO and LUMO energy gap explains the eventual charge transfer interactions taking place within the molecule. The high stability and chemical inertness are due to the presence of high ionization energy. Global chemical descriptors like chemical potential, electrophilicity, hardness, softness, and electronegativity varies the chemical reactivity of the molecule [27–30]. All the calculated parameters indicate the high reactive nature of the grown sample. Also, high electrophilicity values indicate the good electrophile nature of the material [31, 32].

**3.5. Molecular Electrostatic Potential Studies.** Molecular Electrostatic Potential (MEP) is an essential tool for interpreting electrostatic (electron and nuclei) distribution potential and envisage the reactive site of wide ranges in both electrophilic and nucleophilic attacks in chemical reactions,

TABLE 3: Second-order perturbation theory analysis of the Fock matrix in NBO basis for 3M2VPP.

Donor NBO ( <i>i</i> )	Acceptor NBO ( <i>j</i> )	<i>E</i> (2) (kcal/mol)	<i>E</i> ( <i>j</i> )- <i>E</i> ( <i>i</i> ) a.u.	<i>F</i> ( <i>i</i> , <i>j</i> ) a.u.
<i>Within unit 1</i>				
BD * (2)C1-N15	BD * (2) C3-C5	91.12	0.04	0.090
LP (1)C7	BD * (2) C3-C5	71.58	0.14	0.110
LP * (1)C8	BD * (2) C1-N15	67.09	0.10	0.090
BD (2)C3-C5	LP(1) C7	48.58	0.15	0.090
BD (2)C1-N15	LP * (1) C8	43.84	0.21	0.108
BD (2)C3-C5	BD * (2) C1-N15	35.69	0.24	0.084
BD (2)C9-C10	LP * (1) C8	33.67	0.14	0.081
LP * (1)C8	BD * (2) C9-C10	26.13	0.17	0.086
<i>From unit 1 to unit 2</i>				
LP (1)N15	LP * (1) H16	362.82	0.48	0.385
BD (1)C1-N15	LP * (1) H16	14.09	0.98	0.121
BD (1)C8-N15	LP * (1) H16	12.22	0.98	0.113
<i>From unit 2 to unit 3</i>				
LP * (1) H16	BD * (1) O21-P24	4.56	0.26	0.054
<i>From unit 3 to unit 1</i>				
LP (3) O20	BD * (1) C1-H2	4.26	0.67	0.050
<i>From unit 3 to unit 2</i>				
LP (3)O21	LP * (1) H16	114.13	0.48	0.228
LP (1)O21	LP * (1) H16	15.90	0.71	0.108
<i>Within unit 3</i>				
LP (2)O20	BD * (1) O22-P24	22.03	0.49	0.093
LP (3)O20	BD * (1) O21-P24	17.70	0.59	0.092
LP (2)O21	BD * (1) O22-P24	13.22	0.52	0.076
LP (3)O20	BD * (1) O23-P24	11.28	0.49	0.067
LP (2)O20	BD * (1) O23-P24	10.79	0.49	0.065
LP (2)O21	BD * (1) O23-P24	10.52	0.53	0.068
LP (2)O22	BD * (1) O23-P24	10.48	0.57	0.071
LP (2)O23	BD * (1) O22-P24	10.07	0.56	0.069

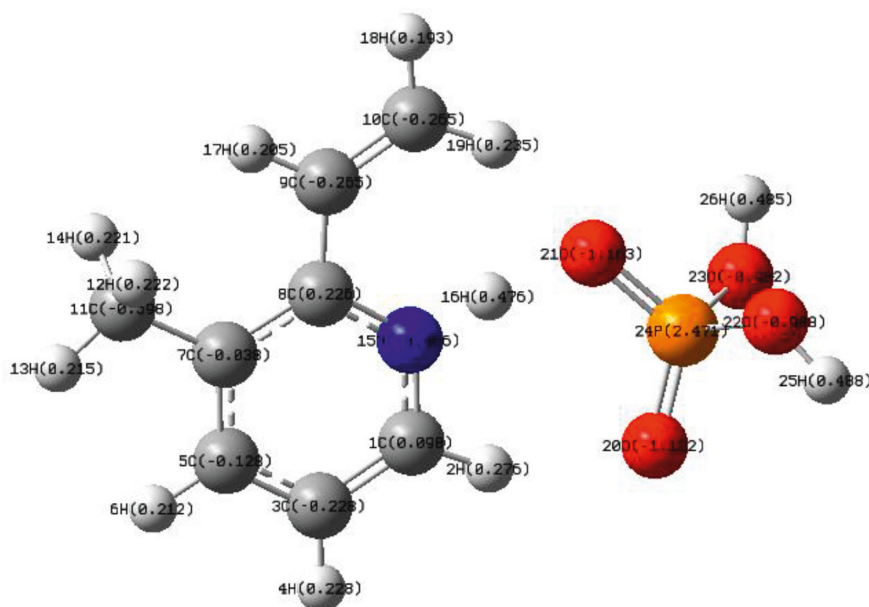


FIGURE 3: NBO charges of 3M2VPP.

and hydrogen-bonding interactions. This map is useful as an indicator of the sites or regions of a molecule to which an approaching electrophile and nucleophile are initially attracted. This is in turn related to the electronic density and

is a very useful descriptor for determining sites for electrophilic attack and related to nucleophilic reactions as well as hydrogen-bonding interactions [33, 34]. The molecular electrostatic potential projection map for 3-methyl 2-vinyl

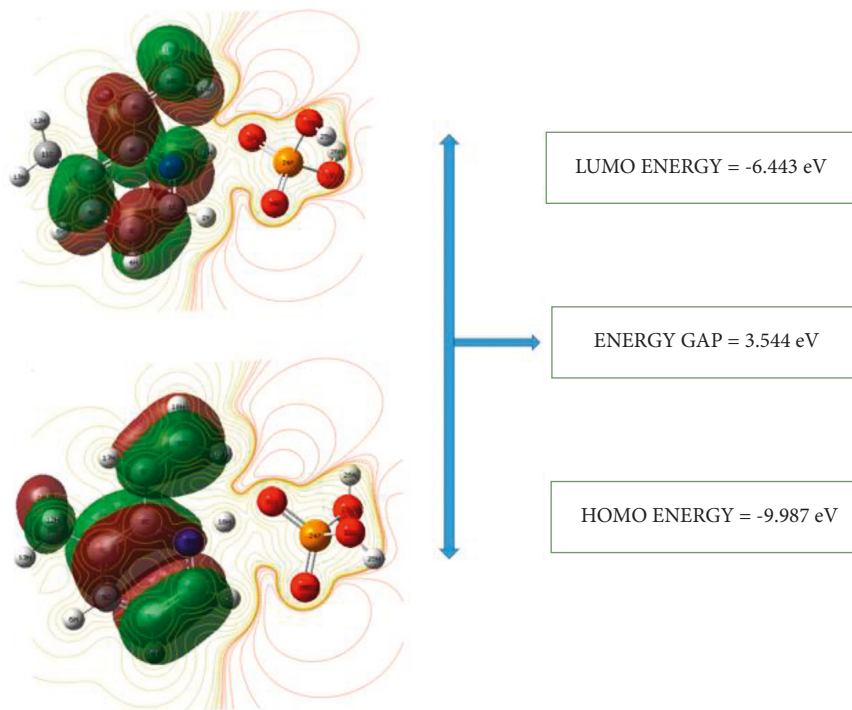


FIGURE 4: HOMO-LUMO plot of 3M2VPP.

TABLE 4: Chemical descriptors of 3M2VPP.

Parameters	Value (eV)
$E_{\text{HOMO}}$	-9.987
$E_{\text{LUMO}}$	-6.443
$\Delta E_{\text{gap}}$	3.544
Ionization potential ( $I$ )	+9.987
Electron affinity ( $A$ )	+6.443
Chemical potential ( $\mu$ )	-8.215
Electronegativity ( $\chi$ )	8.215
Global hardness ( $\eta$ )	1.772
Global softness ( $S$ )	0.282
Electrophilicity ( $\omega$ )	19.042

pyridinium phosphate is calculated using the B3LYP/6-311++G (d, p) method. MEP surface map of 3-methyl 2-vinyl pyridinium phosphate is shown in Figure 5. The reactive sites are located by different colour codes and are highly beneficial to explore the molecular structure with its physiochemical property relationship [35, 36]. Molecular electrostatic potential map ranges from  $-4.324 \times 10^{-2}$  to  $+4.324 \times 10^{-2}$  esu. The total density spectrum ranges from  $4.074 \times 10^{-4}$  to  $+4.074 \times 10^{-4}$  esu. Electrophilic and nucleophilic areas are represented by red and blue colour regions respectively as shown in Figure 6.

**3.6. Nonlinear Optical Properties.** The first-order hyperpolarizability ( $\beta$ ) is a measure of how easily a dipole is induced in a molecule in the presence of an electric field. The first-order hyperpolarizability calculations have been done

using the DFT method based on the finite field approach. The first-order hyperpolarizability is a third-rank tensor that can be described by a  $3 \times 3 \times 3$  matrix. The 27 components of the 3D matrix can be reduced to 10 components due to the Kleinman symmetry [37].

The total induced dipole moment by the applied field is calculated using the Taylor series expansion.

$$\mu = \mu_0 + \alpha_{ij}E_j + \beta_{ijk}E_jE_k + \dots, \quad (1)$$

where  $\alpha$ , linear polarizability;  $\mu_0$ , the permanent dipole moment; and  $\beta_{ijk}$ , first order hyperpolarizability tensor component.

The expression for the static dipole moment is given as

$$\mu = (\mu_x^2 + \mu_y^2 + \mu_z^2)^{1/2}. \quad (2)$$

The following expression gives the isotropic (or average) linear polarizability:

$$\alpha_{\text{Total}} = \frac{(\alpha_{xx} + \alpha_{yy} + \alpha_{zz})}{3}. \quad (3)$$

The magnitude of the first order hyperpolarizability tensor is calculated using the relation,

$$\beta_i = \beta_{iii} + \frac{1}{3} \sum_{i \neq j} (\beta_{ijj} + \beta_{jij} + \beta_{jji}). \quad (4)$$

The output of Gaussian 09W for calculating the magnitude of  $\beta_{\text{Total}}$  is given as follows:

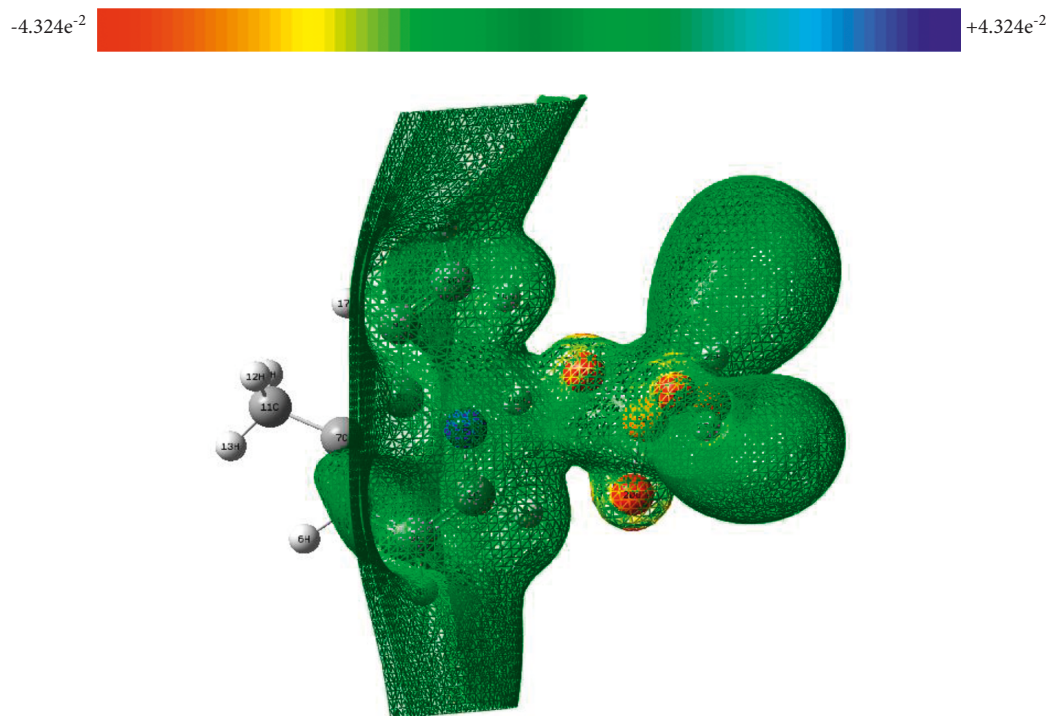


FIGURE 5: MEP map of 3M2VPP.

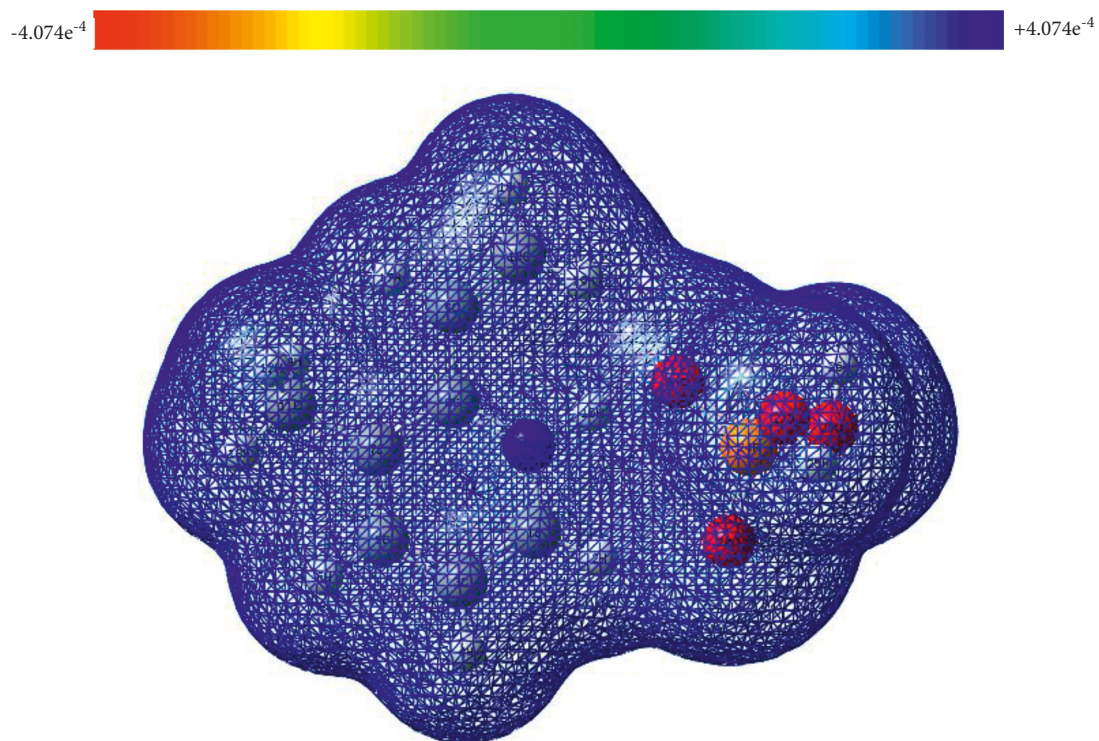


FIGURE 6: Total density spectrum of 3M2VPP.

$$\beta_{\text{Total}} = \sqrt{(\beta_{xxx} + \beta_{xyy} + \beta_{xzz})^2 + (\beta_{yyy} + \beta_{yzz} + \beta_{yxx})^2 + (\beta_{zzz} + \beta_{zxx} + \beta_{zyy})^2}. \quad (5)$$

TABLE 5: Calculated electric dipole moment, polarizability, and first-order hyperpolarizability of 3M2VPP.

Parameters	B3LYP/6-311++G (d, p)	Parameters	B3LYP/6-311++G (d, p)
$\mu_x$	-8.8313	$\beta_{xxx}$	-27.9812
$\mu_y$	1.1298	$\beta_{xxy}$	13.3782
$\mu_z$	0.2376	$\beta_{xyy}$	-21.3378
$\mu$ (D)	8.9064	$\beta_{yyy}$	11.3499
$\alpha_{xx}$	-77.4601	$\beta_{zxx}$	16.8041
$\alpha_{xy}$	7.9872	$\beta_{xyz}$	-17.5345
$\alpha_{yy}$	-83.7978	$\beta_{zyy}$	-4.4329
$\alpha_{xz}$	2.3012	$\beta_{xzz}$	21.2853
$\alpha_{yz}$	-4.0765	$\beta_{yzz}$	-0.2132
$\alpha_{zz}$	-93.5580	$\beta_{zzz}$	1.8827
$\alpha_{tot}$ (esu)	$84.938 \times 10^{-24}$	$\beta_{tot}$ (esu)	$39.878 \times 10^{-31}$

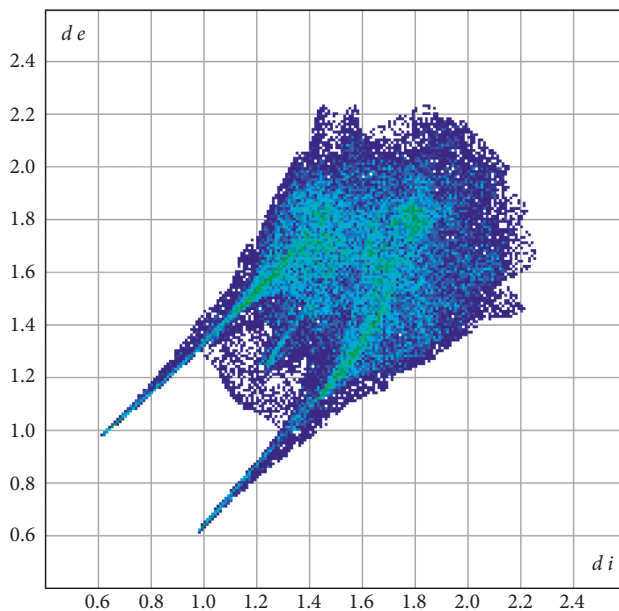
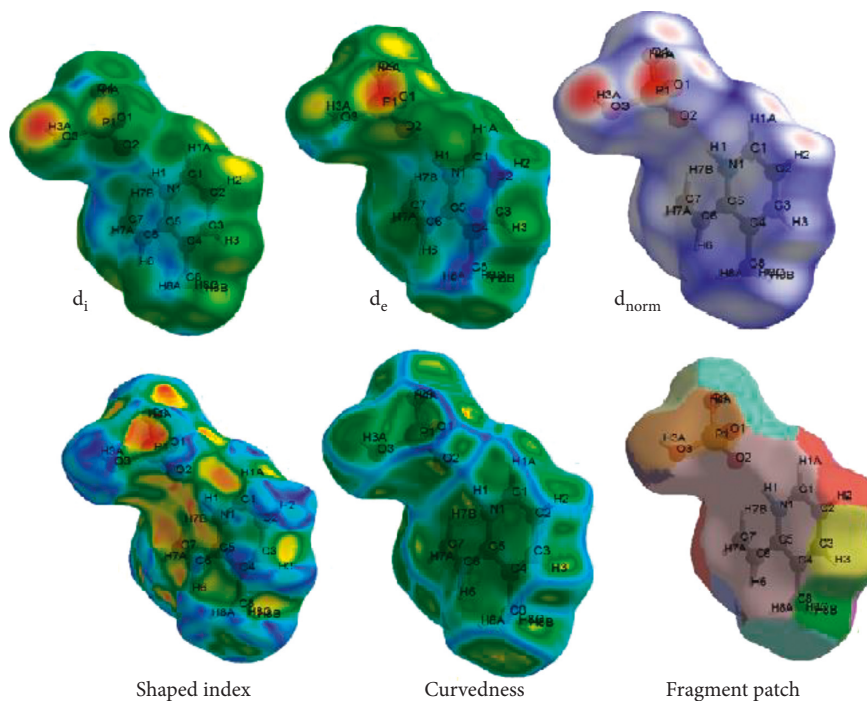


FIGURE 7: Fingerprint of LHLTHH (100%).

FIGURE 8: Hirshfeld surface analysis  $d_i$ ,  $d_e$ ,  $d_{norm}$ , shape index, and curvedness of 3M2VPP.

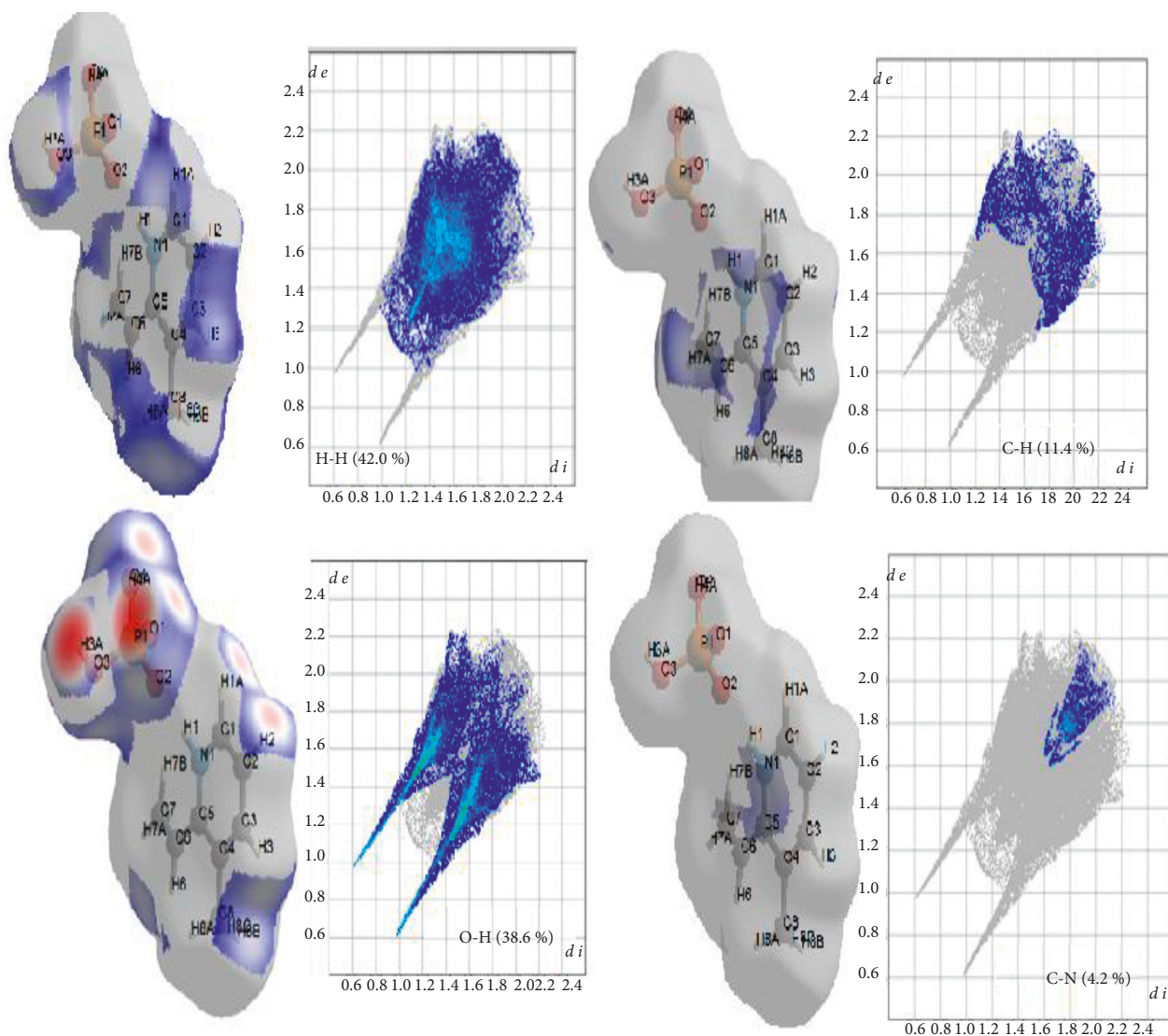


FIGURE 9: Relative contributions to the percentage of Hirshfeld surface area for the various intermolecular contacts in 3M2VPP.

Gaussian 09W program using B3YLP/6-311++G (d, p) methodology to compute first order hyperpolarizability calculations. The total molecular dipole moment ( $\mu$ ), linear polarizability ( $\alpha$ ), and first-order hyperpolarizability ( $\beta$ ) were calculated in atomic units and are converted into electrostatic units. ( $\alpha$ :  $1 \text{ a.u.} = 0.1482 \times 10^{-24} \text{ esu}$ ,  $\beta$ :  $1 \text{ a.u.} = 8.6393 \times 10^{-30} \text{ esu}$ ). Table 5 lists the calculated parameters of an electric dipole moment  $\mu(D)$ , the average polarizability  $\alpha_{tot}$  ( $\times 10^{-24} \text{ esu}$ ), and first-order hyperpolarizability  $\beta_{tot}$  ( $\times 10^{-31} \text{ esu}$ ). The calculated dipole moment is 8.9064 Debye and reveals the ionic nature of the compound. The maximum value of 1.1298 Debye occurs in the Y direction. The maximum hyperpolarizability value is  $21.2852 \times 10^{-31} \text{ esu}$  and it is computed for  $\beta_{zzz}$  direction which is due to the substantial delocalization of electron cloud in that region. The next highest hyperpolarizability is computed to be  $16.8041 \times 10^{-31} \text{ esu}$  and  $11.3499 \times 10^{-31} \text{ esu}$  for the direction  $\beta_{zzx}$  &  $\beta_{yyy}$  respectively. Urea—a well-known standard nonlinear optical material has total polarizability

( $\alpha = 3.8312 \times 10^{-24} \text{ esu}$ ) and first-order hyperpolarizability ( $\beta = 3.7289 \times 10^{-31} \text{ esu}$ ). The total polarizability is computed to be  $39.878 \times 10^{-31} \text{ esu}$ . It is found that 3M2VPP is 10.694 times that of urea and may be expected as a potential candidate for the development of NLO materials [38–42].

**3.7. Hirshfeld Surface Analysis.** CrystalExplorer 3.1 [43] program is used to understand the interactions and the connectivity among the molecules efficiently. The crystallographic information file (.cif) was imported to the crystal explorer to generate the Hirshfeld surfaces. The Hirshfeld surface (HS) is the region around the molecule in the crystal space which can be considered as the boundary separating two regions—the interior (the reference molecule) and the exterior (neighboring molecules) [44]. The 2D fingerprint plot provides a precise two-dimensional graphical representation of the intermolecular interactions in the crystal as shown in Figure 7. The contributions from different contacts to the total Hirshfeld surface area are shown in Figure 8. The

major contribution (42.0%) is from  $H\cdots H$  and (38.6%) from  $O\cdots H$  contacts. The wings are due to the  $C-H\cdots\pi$  interactions. The  $\pi\cdots\pi$  type of interaction is clearly seen on the shape decorated HSs where the characteristic blue and red triangles are present. Hydrogen bonding contacts are represented by red spots which are shown in Figure 8. The  $d_{\text{norm}}$  parameter exhibits a surface with a red-white-blue colour scheme. Bright red spots show the intermolecular contacts less than their vdW radii, while the blue spots show intermolecular contacts longer than their vdW radii. White spots are the sum of their vdW radii. The red regions in Figure 9 are apparent around the phosphor atom participating in the  $P-O\cdots H$  contacts.

#### 4. Conclusion

The compound - 3-methyl 2-vinyl pyridinium phosphate (3M2VPP) was optimized with DFT-B3LYP using a 6-311++G (d, p) basis set. The complete molecular structural parameters of the optimized geometry of the compound have been obtained from DFT calculations. The calculated bond length, bond angle, and dihedral angles are compared with the XRD data of 3M2VPP. All the experimental and theoretical data are in a good agreement with each other. The vibrational frequencies of the fundamental modes of the compound have been precisely assigned, and analysed and the theoretical results are provided with a clear assignment description. The electronic properties such as highest occupied molecular orbital (HOMO) and lowest unoccupied molecular orbital (LUMO) energies are determined by the B3LYP/6-311++G (d, p) basis set. The calculated HOMO-LUMO energy gap of 3.544 eV reveals that the molecule possesses good kinetic stability and low chemical reactivity. Further global chemical descriptors explain the possible reactive sites and provide a firm explanation for the reactivity of the 3M2VPP molecule. The intramolecular charge transfer and hyper-conjugative interaction of the compound are investigated from natural bonding orbitals (NBOs) analysis. The highest intramolecular stabilization energy of 91.12 kJmol<sup>-1</sup> is found in 3-methyl-2-vinylpyridine between antibonding  $\pi$  orbitals of the atoms C1-N15 to C3-C5. The strongest intermolecular stabilization energy between lone pair of electronegative nitrogen atom N15 in 3-methyl-2-vinyl pyridine to H16 phosphoric acid establishes with an energy of 362.82 kJmol<sup>-1</sup> and lone pair of oxygen atom O21 with antibonding H16 has the energy 114.13 kJmol<sup>-1</sup> confirms the protonation occurrence between the molecules. Intramolecular stabilization energy of phosphoric acid lies in the range of 10 to 22 kJmol<sup>-1</sup>. Molecular electrostatic potential envisages the presence of reactive sites of both electrophilic and nucleophilic reactions. The calculated first-order hyperpolarizability of 3M2VPP is 10.694 times greater than that of urea and may be expected as a potential candidate for the development of NLO materials. Hirshfeld surface analysis was performed to determine the intermolecular interactions and the crystal packing. Hirshfeld surface

analysis shows  $H\cdots H$  (42.0%) followed by  $O\cdots H$  (38.6%) as a major contribution towards crystal surface. All the above results confirm the potential candidature of the chosen material for optoelectronic and photonic applications.

#### Data Availability

The authors confirm that the data supporting the findings of this study are available within the article.

#### Conflicts of Interest

The authors report there are no conflicts of interest.

#### References

- [1] J. Williams David, "Nonlinear optical properties of organic and polymeric materials," in *ACS Symposium Series* American Chemical Society, Washington, D.C., USA, 1983.
- [2] D. S. Chemla and J. Zyss, *Nonlinear Optical Properties of Organic Molecules and Crystals*, Academic Press, Cambridge, MA, USA, 1987.
- [3] H. B. Yahia, S. Sabri, R. Essehli et al., "Crystal growth, single crystal structure, and biological activity of thiazolo-pyridine dicarboxylic acid derivatives," *ACS Omega*, vol. 5, no. 43, pp. 27756–27765, 2020.
- [4] H. Soscún, O. Castellano, Y. Bermúdez, C. Toro-Mendoza, A. Marcano, and Y. Alvarado, "Linear and nonlinear optical properties of pyridine N-oxide molecule," *Journal of Molecular Structure: Theochem*, vol. 592, no. 1–3, pp. 19–28, 2002.
- [5] S. Gowri, T. Uma Devi, S. Alen, D. Sajan, C. Surendra Dilip, and G. Vinitha, "Synthesis, crystal structure, optical and third order nonlinear optical properties of phosphoric acid pyridine-1-ium-2-carboxylate," *Journal of Materials Science: Materials in Electronics*, vol. 29, no. 23, pp. 19710–19723, 2018.
- [6] M. Moreno Oliva, J. Casado, J. T. López Navarrete, G. Hennrich, M. C. Ruiz Delgado, and J. Orduna, "Linear and nonlinear optical properties of pyridine-based octopolar chromophores designed for chemical sensing joint spectroscopic and theoretical study," *Journal of Physical Chemistry C*, vol. 111, no. 50, pp. 18778–18784, 2007.
- [7] R. Sapale Seema and N. A. Borade, "Nonlinear optical properties (NLO) study of some novel fluorescent 2-chloroimidazo (1,2-A) pyridine derivatives," *European Journal of Molecular & Clinical Medicine*, vol. 7, no. 11, pp. 4529–4539, 2021.
- [8] T. Haruhiko, T. Hirano, S. Saito, T. Mutai, and K. Araki, "Substituent effects on fluorescent properties of imidazo (1, 2-A) pyridine-based compounds," *Bulletin of the Chemical Society of Japan*, vol. 72, no. 6, pp. 1327–1334, 1999.
- [9] V. B. Kovalska, M. Losytskyy, D. V. Kryvorotenko, A. O. Balanda, V. P. Tokar, and S. M. Yarmoluk, "Synthesis of novel fluorescent styryl dyes based on the imidazo (1, 2-A) pyridinium chromophore and their spectral-fluorescent properties in the presence of nucleic acids and proteins," *Dyes and Pigments*, vol. 68, no. 1, pp. 39–45, 2006.
- [10] D. Firmansyah, A. I. Ciuciu, V. Hugues, M. Blanchard-Desce, L. Flamigni, and D. T. Gryko, "Bright, fluorescent dyes based on imidazo (1, 2-A) pyridines that are capable of two-photon absorption," *Chemistry-An Asian Journal*, vol. 8, no. 6, pp. 1279–1294, 2013.

- [11] S. Sowmiah, J. M. S. S. Esperança, L. P. N. Rebelo, and C. A. M. Afonso, "Pyridinium salts: from synthesis to reactivity and applications," *Organic Chemistry Frontiers*, vol. 5, no. 3, pp. 453–493, 2018.
- [12] W. Śliwa, *N-Substituted Salts of Pyridine and Related Compounds*, WSP, Montreal, Canada, 1996.
- [13] G. Kalaiselvi, V. Sabari, S. Balasubramanian, and S. Aravindhan, "3-methyl-2-vinylpyridinium phosphate," *Acta Crystallographica Section E Structure Reports Online*, vol. 69, no. 4, 2013.
- [14] M. J. Frisch, G. W. Trucks, H. B. Schlegel et al., *Gaussian 09, Revision D. 01*, Gaussian, Inc, Wallingford, CT, USA, 2013.
- [15] R. Dennington, T. Keith, and J. Millam, "GaussView, version 5," 2009, [https://www.gaussian.com/g\\_tech/gv5ref/gv5citation.htm](https://www.gaussian.com/g_tech/gv5ref/gv5citation.htm).
- [16] E. Vaganova, M. Rozenberg, F. Dubnikova, D. Danovich, and S. Yitzchaik, "Acidity of the methyne group of poly (4-vinylpyridine) leads to side-chain protonation in pyridine," *New Journal of Chemistry*, vol. 39, no. 8, pp. 5920–5922, 2015.
- [17] V. Koleva and V. Stefov, "Phosphate ion vibrations in dihydrogen phosphate salts of the type M (H<sub>2</sub>PO<sub>4</sub>) 2·2H<sub>2</sub>O (M = Mg, Mn, Co, Ni, Zn, Cd): spectra-structure correlations," *Vibrational Spectroscopy*, vol. 64, pp. 89–100, 2013.
- [18] V. Videnova-Adrabińska, W. Wojciechowski, and J. Baran, "Polarized infrared and Raman spectra of monoclinic CsH<sub>2</sub>PO<sub>4</sub> single crystal and its deuterated homologue CsD<sub>2</sub>PO<sub>4</sub>: part II. internal vibrations of the PO<sub>4</sub> ion," *Journal of Molecular Structure*, vol. 156, no. 1-2, pp. 15–27, 1987.
- [19] B. Marchon and A. Novak, "Vibrational study of CsH<sub>2</sub>PO<sub>4</sub> and CsD<sub>2</sub>PO<sub>4</sub> single crystals," *The Journal of Chemical Physics*, vol. 78, no. 5, pp. 2105–2120, 1983.
- [20] V. Videnova-Adrabińska and J. Baran, "Vibrational study of (NH<sub>4</sub>)<sub>2</sub>HPO<sub>4</sub> and (ND<sub>4</sub>)<sub>2</sub>DPO<sub>4</sub> single crystals. the PO<sub>4</sub> ion vibration couplings," *Journal of Molecular Structure*, vol. 175, pp. 295–302, 1988.
- [21] E. D. Glendening, A. E. Reed, J. E. Carpenter, and F. Weinhold, *NBO, Version 3.1*, Gaussian Inc, Pittsburgh, PA, USA, 2003.
- [22] M. Khalid, A. Ali, S. Haq et al., "O-4-acetyl-amino-benzene-sulfonylated pyrimidine derivatives: synthesis, SC-XRD, DFT analysis and electronic behaviour investigation," *Journal of Molecular Structure*, vol. 1224, Article ID 129308, 2021.
- [23] M. Khalid, A. Ali, M. Adeel et al., "Facile preparation, characterization, SC-XRD and DFT/DTDFT study of diversely functionalized unsymmetrical bis-aryl- $\alpha$ ,  $\beta$ -unsaturated ketone derivatives," *Journal of Molecular Structure*, vol. 1206, Article ID 127755, 2020.
- [24] M. Khalid, M. N. Arshad, M. N. Tahir et al., "An efficient synthesis, structural (SC-XRD) and spectroscopic (FTIR, <sup>1</sup>HNMR, MS spectroscopic) characterization of novel benzofuran-based hydrazones: an experimental and theoretical studies," *Journal of Molecular Structure*, vol. 1216, Article ID 128318, 2020.
- [25] M. Khalid, A. Ali, S. Abid et al., "Facile ultrasound-based synthesis, SC-XRD, DFT exploration of the substituted acyl-hydrazones: an experimental and theoretical slant towards supramolecular chemistry," *Chemistry Select*, vol. 5, no. 47, pp. 14844–14856, 2020.
- [26] K. Fukui, "Role of frontier orbitals in chemical reactions," *Science*, vol. 218, no. 4574, pp. 747–754, 1982.
- [27] R. G. Parr, L. V. Szentpály, and S. Liu, "Electrophilicity index," *Journal of the American Chemical Society*, vol. 121, no. 9, pp. 1922–1924, 1999.
- [28] P. K. Chattaraj, B. Maiti, and U. Sarkar, "Philicity: a unified treatment of chemical reactivity and selectivity," *The Journal of Physical Chemistry A*, vol. 107, no. 25, pp. 4973–4975, 2003.
- [29] N. Dege, H. Gokce, O. E. Doğan et al., "Quantum computational, spectroscopic investigations on N-(2-(2-chloro-4,5-dicyanophenyl)amino)ethyl)-4-methylbenzenesulfonamide by DFT/TD-DFT with different solvents, molecular docking and drug-likeness researches," *Colloids and Surfaces A Physicochemical and Engineering Aspects*, vol. 638, Article ID 128311, 2022.
- [30] A. Bendjeddou, T. Abbaz, A. Gouasmia, and D. Villemin, "Studies on chemical reactivity of p-aminophenyl benzene-fused bis tetrathiafulvalenes through quantum chemical approaches," *American Journal of Applied Chemistry*, vol. 4, no. 3, pp. 104–110, 2016.
- [31] A. A. Abdulridha, M. A. Albo Hay Allah, S. Q. Makki, Y. Sert, H. E. Salman, and A. A. Balakit, "Corrosion inhibition of carbon steel in 1 M H<sub>2</sub>SO<sub>4</sub> using new Azo Schiff compound: electrochemical, gravimetric, adsorption, surface and DFT studies," *Journal of Molecular Liquids*, vol. 315, Article ID 113690, 2020.
- [32] A. A. Balakit, S. Q. Makki, Y. Sert et al., "Synthesis, spectrophotometric and DFT studies of new Triazole Schiff bases as selective naked-eye sensors for acetate anion," *Supramolecular Chemistry*, vol. 32, no. 10, pp. 519–526, 2020.
- [33] S. Eolo and J. Tomasi, "Electronic molecular structure, reactivity and intermolecular forces: an heuristic interpretation by means of electrostatic molecular potentials," in *Advances in Quantum Chemistry* Academic Press, Cambridge, MA, USA, 1978.
- [34] N. Swarnalatha, S. Gunasekaran, M. Nagarajan, S. Srinivasan, G. Sankari, and G. R. Ramkumaar, "Vibrational, UV spectra, NBO, first order hyperpolarizability and HOMO–LUMO analysis of carvedilol," *Spectrochimica Acta Part A: Molecular and Biomolecular Spectroscopy*, vol. 136, pp. 567–578, 2015.
- [35] M. Khalid, M. A. Ullah, M. Adeel et al., "Synthesis, crystal structure analysis, spectral IR, UV–Vis, NMR assessments, electronic and nonlinear optical properties of potent quinoline based derivatives: interplay of experimental and DFT study," *Journal of Saudi Chemical Society*, vol. 23, no. 5, pp. 546–560, 2019.
- [36] M. Khalid, A. Ali, S. Asim et al., "Persistent prevalence of supramolecular architectures of novel ultrasonically synthesized hydrazones due to hydrogen bonding (X–H–O; X = N): experimental and density functional theory analyses," *Journal of Physics and Chemistry of Solids*, vol. 148, Article ID 109679, 2021.
- [37] D. A. Kleinman, "Nonlinear dielectric polarization in optical media," *Physical Review*, vol. 126, pp. 1977–1979, 1962.
- [38] N. Kanagathara, R. Usha, V. Natarajan, and M. K. Marchewka, "Molecular geometry, vibrational, NBO, HOMO–LUMO, first order hyper polarizability and electrostatic potential studies on anilinium hydrogen oxalate hemihydrate—an organic crystalline salt," *Inorganic and Nano-Metal Chemistry*, vol. 52, no. 2, pp. 226–233, 2022.
- [39] S. Muthu and S. Renuga, "Vibrational spectra and normal coordinate analysis of 2-hydroxy-3-(2-methoxyphenoxy) propyl carbamate," *Spectrochimica Acta Part A: Molecular and Biomolecular Spectroscopy*, vol. 132, pp. 313–325, 2014.
- [40] M. Khalid, H. M. Lodhi, M. U. Khan, and M. Imran, "Structural parameter-modulated nonlinear optical amplitude of acceptor– $\pi$ –D– $\pi$ –donor-configured pyrene derivatives: a DFT approach," *RSC Advances*, vol. 11, no. 23, pp. 14237–14250, 2021.

- [41] M. Khalid, A. Ali, R. Jawaria et al., "First principles study of electronic and nonlinear optical properties of A-D- $\pi$ -A and D-A-D- $\pi$ -A configured compounds containing novel quinoline-carbazole derivatives," *RSC Advances*, vol. 10, no. 37, pp. 22273–22283, 2020.
- [42] M. Khalid, M. U. Khan, I. Shafiq et al., "NLO potential exploration for D- $\pi$ -A heterocyclic organic compounds by incorporation of various  $\pi$ -linkers and acceptor units," *Arabian Journal of Chemistry*, vol. 14, no. 8, Article ID 103295, 2021.
- [43] S. K. Wolff, D. J. Grimwood, J. J. McKinnon, M. J. Turner, D. Jayatilaka, and M. A. Spackman, *Crystal Explorer 3.1*, University of Western Australia, Crawley, Western Australia, 2013.
- [44] M. A. Spackman and D. Jayatilaka, "Hirshfeld surface analysis," *CrystEngComm*, vol. 11, no. 1, pp. 19–32, 2009.